Biomaterials Science

ROYAL SOCIETY OF CHEMISTRY

PAPER

View Article Online
View Journal | View Issue

Cite this: *Biomater. Sci.*, 2022, **10**, 2706

Dendron-functionalised hyperbranched bis-MPA polyesters as efficient non-viral vectors for gene therapy in different cell lines†

María San Anselmo, [a] Alejandro Postigo, [a] Alexandre Lancelot, [a] José Luis Serrano, [a] Teresa Sierra *[a] and Silvia Hernández-Ainsa *[a,b]

Gene therapy has become a relevant tool in the biomedical field to treat or even prevent some diseases. The effective delivery of genetic material into the cell remains a crucial step to succeed in this purpose. In the search for efficient non-viral vectors, a series of amino-terminated dendronized hyperbranched polymers (DHPs) of different generations based either on bis-MPA or bis-GMPA have been designed. All of them have demonstrated an accurate ability to complex two types of genetic materials, a plasmid DNA and a siGFP, yielding dendriplexes. Moreover, some of them have proved to be able to deliver the genetic material inside the cells, resulting in the effective accomplishment of the desired genetic modification and improving the activity of some commercial transfection reagents. Different cell lines, including cancer and mesenchymal stem cells, have been studied here to evaluate the ability of DHPs as vectors for transfection. Treatments based on mesenchymal stem cells are gaining importance due to their pluripotency. Thus, it is of special relevance to introduce a genetic modification into a mesenchymal cell line as it allows it to act over a wide spectrum of tissues after inducing cellular differentiation.

Received 11th March 2022,
Accepted 30th March 2022

DOI: 10.1039/d2bm00365a

rsc.li/biomaterials-science

Introduction

The development of ingenious methodologies to deliver genetic material inside the cells of interest has considerably improved the efficacy of gene therapy–based treatments. Physical methods such as electroporation, ultrasound, hydrodynamics, needle injection or gene gun immunisation are included among the various approaches studied mostly for *ex vivo* applications,[1,2] whereas for *in vitro* and *in vivo* purposes, the biggest attention is focused on chemical-based vectors for gene delivery as they protect nucleic acids from degradation and define complexes suitable for cell internalisation.[3] A wide range of viral vectors have been explored as genetic materials.[4] Some of them have received clinical approval,[5] but yet they present some limitations related to the immune response provoked in the host tissues,[6] its safety and some manufacturing limits.[3]

Non-viral vectors constitute an alternative method to mediate gene delivery by overcoming those undesired aspects, although their transfection efficiency can be compromised due to the endocytosis process by which they enter living cells.[7] Among them, lipoplexes or polyplexes, formed by the electrostatic interactions between cationic lipids or polymers, respectively, with the nucleic acids are the most widely explored.[8] These cationic vectors exhibit versatility in the type and size of genetic material complexation and in the attachment of specific targeting ligands. Some cationic polymers studied as non-viral gene delivery systems include polyamines like poly(ethylenimine) (PEI) derivatives, polyesters like poly-DL-lactide (PLA), polysaccharides like chitosan or pectin, polypeptides like poly-L-lysine (PLL) or structurally controlled dendrimers.[7–9] The low polydispersity exhibited by dendrimers and the possibility to functionalise them with diverse ligands on the surface[10] postulate them as promising candidates for gene therapy.[11] Some recent successful examples include dendrimers based on poly(amidoamine) (PAMAM),[12] poly(propylene imine) (PPI),[13] polyesters (2,2′-bis(hydroxymethyl)propionic acid, bis-MPA)[14] and polyesteramides (2,2′-bis(glycyloxymethyl)propionic acid, bis-GMPA),[15] and carbosilane,[16] ornithine,[17] guanidinylated,[18] phosphorous[19] or triazine[20] containing dendrimers.

The attachment of dendrons to a hyperbranched core yielded dendronized hyperbranched polymers (DHPs) which allowed us to obtain large molecules with a high number of amino-terminal groups in a feasible way. This strategy

[a]*Instituto de Nanociencia y Materiales de Aragón (INMA), CSIC-Universidad de Zaragoza, Zaragoza, Spain. E-mail: silviamh83@unizar.es, tsierra@ctq.csic.es*
[b]*ARAID Foundation, Government of Aragón, Zaragoza, Spain*

†Electronic supplementary information (ESI) available: Further synthetic protocols and characterisation of the compounds as well as further transfection data. See DOI: https://doi.org/10.1039/d2bm00365a

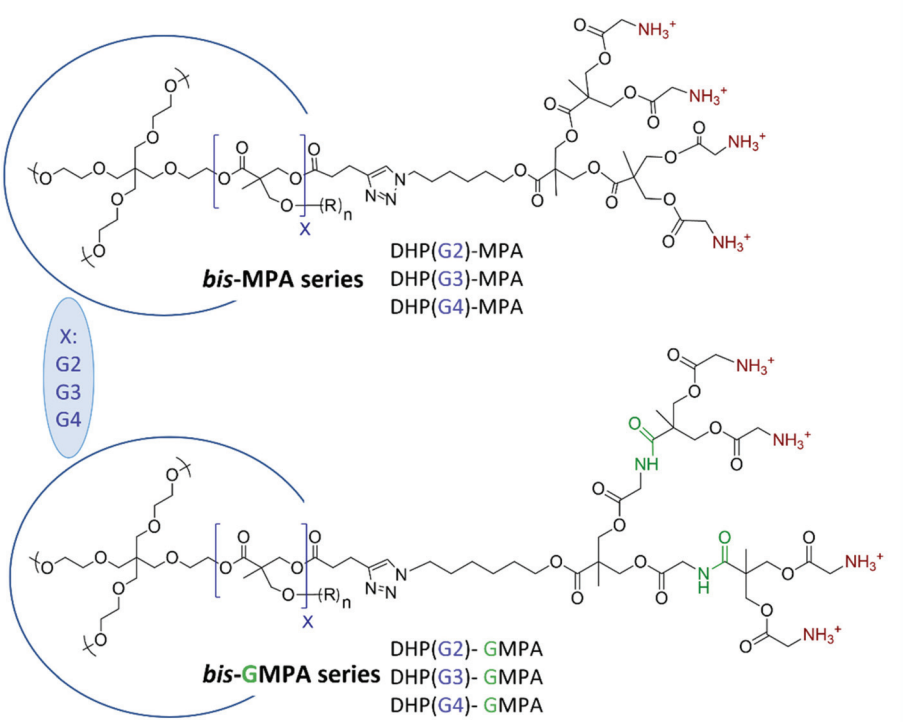

Fig. 1 Chemical structures of the two series of DHPs: a hyperbranched polyester core of different generations (G2, G3 or G4) covalently linked to dendrons of polyester (bis-MPA series, above) or polyester amide (bis-GMPA series, below) (note that the amide groups are marked in green and ammonium groups in red). As detailed in the text (DHPs characterization section) and in the ESI (Table S1†), a small average number of residual groups (*n*), namely R = OH and/or R = $-COCH_2CH_2C{\equiv}C$ can be present in the final DHP depending on the generation of the HP core and the nature of the dendron, either bis-MPA or bis-GMPA.

employed for the synthesis of DHPs rendered structures with similar properties to those of high generation dendrimers with the advantage of a lower synthesis effort required.[14,21,22] In this regard, DHP derivatives consisting of hyperbranched cores of an hyperbranched commercial polyester core of bis-MPA of generations 2, 3 and 4 decorated with bis-MPA dendrons of generation 3 have been previously synthesised by taking advantage of the 1,3-dipolar cycloaddition click chemistry (CuAAC).[14] Their biocompatibility and their terminal polyamine composition enabled them to complex a plasmid DNA and to transfect it into mesenchymal cells at levels comparable to commercial transfectants.[14]

In the present work, we aim to elucidate whether the substitution of bis-MPA dendrons with bis-GMPA ones has an impact on the transfection efficiency of the resulting DHPs. In this line, the presence of inner amides in the bis-GMPA structure introduces hydrogen bonds that can modify the compactness of the DHPs and consequently the disposition of external amine groups and their interaction with the genetic material. With this objective, two series of homologous DHPs comprising three generations of the hyperbranched core (G2, G3 and G4) and bearing either bis-MPA or bis-GMPA dendrons of generation 2 have been prepared. The bis-MPA series includes DHP(G2)-MPA, DHP(G3)-MPA and DHP(G4)-MPA and, on the other hand, the bis-GMPA series includes DHP(G2)-GMPA, DHP(G3)-GMPA and DHP(G4)-GMPA (Fig. 1). To evaluate their gene transfection ability, two different types of genetic materials were employed to express or silence the expression of a specific protein as a proof of concept, namely, pGFP, a plasmid DNA, and siGFP, a small interference RNA (siRNA) molecule. In addition, the potential of the mesenchymal stem cells (MSCs) to differentiate into numerous cell types has pointed them as a powerful tool to act over different tissues raising their value in the biomedical field of regenerative medicine and oncology.[23] Consequently, its use as gene therapy host cells is evaluated in this work and compared with the tumoral cell line HeLa.

Experimental section

Materials

All the chemical reagents were purchased from Sigma Aldrich or Acros Organics and the solvents from Fisher Scientific or Scharlab. The plasmid DNA employed was the pAcGFP1-N1 vector (Clontech), abbreviated as pGFP, of 4.7 kb, which encodes a GFP from *Aequorea coerulescens* (excitation maximum = 475 nm; emission maximum = 505 nm). Among its characteristics, this vector contains a multiple cloning site that allows gene fusions to the AcGFP1 gene at the

N-terminus, yielding a fusion protein that maintains the fluorescent properties. The small interference RNA selected to silence GFP in those lines expressing the protein was the GFP Duplex I (Horizon, Dharmacon), hereinafter named siGFP. Superfect and Lipofectamine 3000 were purchased from Qiagen and Invitrogen, respectively.

Plasmid DNA preparation and purification

The commercial pAcGFP1-N1 plasmid was transformed into *Escherichia coli* DH5α and propagated in LB medium with kanamycin, firstly in LB agar overnight at 37 °C to obtain isolated colonies and then, the selected colonies were grown in liquid LB for 24 hours at 37 °C. Then, plasmid DNA was purified with a PureLink Expi Endotoxin-Free Maxi Plasmid Purification Kit (ThermoFisher). Digestion with the restriction enzyme NotI (ThermoFisher) followed by gel electrophoresis (0.8% agarose) was performed to evaluate the extracted plasmid purity. Its concentration was spectroscopically determined using an ND1000 spectrophotometer.

DHPs: synthesis and characterisation

DHP synthesis. The synthesis of DHPs involved three main stages: procedure (I) alkyne functionalisation of commercial hyperbranched polyesters, procedure (II) azide–alkyne cycloaddition (CuAAC) of the corresponding *t*-Boc protected dendron and procedure (III) final cleavage of *t*-Boc ending groups (see the ESI, section S1†). In addition, rhodamine B-labelled DHPs were prepared by covalent bonding of a small amount of the fluorophore to the terminal amino groups of the DHPs already synthesised (see the ESI, section S2†). Specifically, the amount of RhB added was estimated to render a final functionalisation of around 1% of the amino terminal groups of each DHP. The synthesis of the constituent dendrons N_3-[MPA,G2]-$(NHBoc)_4$ [24] and N_3-[GMPA,G2]-$(NHBoc)_4$ [15] was previously described by our group for the construction of various dendritic structures with different biomedical purposes.

DHPs characterisation. ^{1}H nuclear magnetic resonance (^{1}H NMR) and ^{13}C NMR experiments were performed using a Bruker AV-400 (^{1}H: 400 MHz, ^{13}C: 100 MHz) spectrometer using deuterated chloroform ($CDCl_3$) or deuterated methanol (CD_3OD) as the solvent. The chemical shifts are given in ppm relative to TMS and the coupling constants are given in Hz; the residual solvent peak was used as the internal standard. The infrared (IR) spectra were obtained using an FTIR ATI-Mattson Genesis Series II or a JASCO FT/IR-4100 apparatus and recorded between 4000 and 600 cm^{-1}. The measurements were performed in the attenuated total reflection (ATR) mode. Size exclusion chromatography (SEC) was performed using a Waters e2695 Alliance system employing two in series Styragel columns HR4 and HR1 (500 and 104 Å pore size) and a Waters 2424 evaporation light-scattering detector with a sample concentration of 1 mg mL^{-1}. The solvent was THF (HPLC grade) with a flow rate of 1 mL min^{-1} at 35 °C; poly(methyl methacrylate) (PMMA) was used as the standard for calibration.

Transmission electron microscopy

Electron microscopy images were recorded using an FEI TECNAI T20 system with a beam power of 200 kV. A droplet (10 μL) of the freshly prepared sample at 1 mg mL^{-1} was deposited on a formvar (10 nm)/carbon film (1 nm) coated with a 400 mesh copper grid (ANAME), and 1% aqueous uranyl acetate solution was used as a negative stain.

For cryogenic TEM, lacey carbon film 300 mesh copper grids were previously ionised. A droplet of the freshly prepared sample was deposited on the grid. Sample vitrification was automatically processed using a vitrobot (FEI) and performed in liquid ethane. A specific sample holder, Gatan for cold samples, was used to stock the grids in liquid nitrogen for sample vitrification prior to observation with the microscope.

Dendriplexes formation and characterisation

Dendriplexes were freshly formed before each experiment. DHPs and nucleic acids were softly mixed by pipetting in serum free DMEM (Dulbecco's Modified Eagle Medium) medium (SFM). Then, they were incubated for 20 minutes at room temperature. Different N/P ratios were assayed to establish the minimum amount of dendritic material needed to complex a fixed amount of genetic material (0.2 μg of pGFP and 0.225 μg of siGFP). The number of N^+ terminal groups of each molecule of DHP and the P^- groups of the nucleic acids were considered in N/P ratio determination. Lipofectamine™ 3000 (Invitrogen) and SuperFect® (Qiagen) were employed as control transfection reagents of different chemical nature, the first one being a commonly used lipid transfection reagent whereas the second one is based on a dendritic globular structure more similar to the DHPs here described.

Gel retardation assay

A gel retardation assay was performed in order to check the complete nucleic acid complexation. 0.8% (w/v) agarose gels stained with 3 μL of GelRed were prepared in 1× TAE buffer. Different N/P ratios were assayed with a fixed amount of nucleic acid and increasing amounts of DHP in a total volume of 12 μL of SFM. Specifically, 0.2 μg of pGFP and 0.225 μg of siGFP were fixed considering commercial recommendations and the sensitivity of the technique. Electrophoresis was run at 90–100 V for 20–30 min and a GelDoc (Bio-Rad) was employed to visualise the gels.

Dynamic light scattering

The hydrodynamic diameters of the aggregates (empty DHPs and dendriplexes) were determined by dynamic light scattering (DLS) measurements using a Malvern Instruments Nano ZS. Dendriplexes were prepared in distilled water, fixing the concentrations of pGFP at 20 μg mL^{-1} and siGFP at 5.7 μg mL^{-1}. DHP concentrations ranged from 0.5 to 11.3 mg mL^{-1} to establish the N/P ratios of 25 or 500 for pGFP and 150 or 750 for siGFP, the ones at which the complexes are completely formed and the most effective ones in terms of transfection activity. Empty DHPs were prepared at 0.5 mg mL^{-1} under the same

conditions. In all cases, complexes were formed by incubating for 20 minutes at room temperature. Disposable cuvettes were employed and a series of three measurements were performed per sample. Hydrodynamic diameters (in nm) are obtained by the size distributions measured in number and intensity.

ζ potential titration

Measurements were performed using Malvern Instruments Nano ZS in PBS buffer of pH 7.4. Samples were prepared with 1 μg mL^{-1} of pGFP and 0.3 μg mL^{-1} of siGFP, with DHPs ranging from 26.3 to 565 μg mL^{-1} to form the same N/P ratios described for DLS measurements. The complexes were softly mixed and incubated for 20 minutes at room temperature. Three measurements were performed per sample.

Atomic force microscopy

Atomic force microscopy (AFM) measurements were carried out using a Veeco-Bruker Multimode 8 instrument using a cantilever with a force constant of 22–100 N m^{-1} (NT-NMD Spectrum Instruments). 4 μL of samples in distilled water were deposited into previously exfoliated mica substrate and allowed to fix for 5 minutes. Then, three consecutive washes with milliQ water were performed and the samples were softly dried with N_2 flux for 3 minutes. The soft tapping mode in air was employed for the measurements (150–800 kHz) and the software WSxM 4.0 Beta 9.3[25] was used for further image analysis.

Cell lines and culture

Cervical carcinoma cell line HeLa (obtained from Cancer Research-UK Cell Services) and HeLa-GFP, transformed to intrinsically express the GFP protein, were grown in DMEM (high glucose with L-glutamine) supplemented with 10% FBS (fetal bovine serum), and 1% antibiotics (penicillin, streptomycin, amphotericin) at 37 °C and 5% CO_2 under a humidified atmosphere. Mesenchymal stem cells from mouse (mMSCs) from C57BL/6 strain and those stably expressing GFP, mMSCs-GFP, were maintained under the same experimental conditions with their specific MesenCult™ Expansion Medium for mice (StemCell Technologies Inc) supplemented with L-glutamine.

Viability assay

The evaluation of the cytotoxic effect of the compounds was carried out by the Alamar Blue assay. Briefly, the cells were seeded at a density of 1×10^4 cells per well in 96 multiwell culture plates and after 24 hours of incubation at 37 °C, the medium was replaced by 50 μL of the testing compounds dissolved in SFM per well, in triplicates. After 4, 8 or 24 h of incubation, the solutions were removed and 100 μL of fresh complete medium were added and incubated for another 48 hours. After that, the medium was replaced by a 10% (v/v) Alamar Blue dye solution in complete DMEM and allowed to react for 2 hours at 37 °C. Then, absorbance at 570 and 600 nm was read using a Multiskan GO (ThermoScientific) plate reader.

Transfection experiments

For pGFP transfection, HeLa or mMSCs cells were seeded at a density of 1×10^4 cells per well in 96 multiwell culture plates in their respective culture medium. After 24 h of incubation at 37 °C, the culture medium was removed and 50 μL of dendriplexes already formed in SFM as described above were added per well in triplicate. 0.2 μg of pGFP per well was added in all the cases while the amount of dendrimer was adjusted to cover a wide range of N/P ratios (25, 50, 100, 250, and 500). The complexes were incubated for 4, 8 or 24 h at 37 °C and then the compounds were replaced with 100 μL of fresh medium. After 48 h of incubation, GFP expression was evaluated by fluorescence microscopy (NIS-Elements, Nikon) and quantified by fluorimetric determination at excitation and emission wavelengths of 485/20 and 516/20 using a microplate reader (Synergy HT). Transfection experiments with siGFP were similarly performed with HeLa-GFP and mMSCs-GFP cell lines, establishing 200 nM as the fixed concentration of siGFP per well. N/P ratios tested were 150, 300, 500 and 750. Finally, the GFP-expression decrease was determined following the same procedures. For positive controls, the commercial reagents Lipofectamine 3000 and SuperFect were incubated with nucleic acids at the corresponding ratios previously established by following the supplier recommendations. Naked nucleic acids were also tested under the same concentrations and no treated cells were included as negative controls for transfection experiments.

Internalisation and intracellular distribution

To evaluate the intracellular distribution of the rhodamine labelled DHPs with pGFP, they were visualised by confocal laser scanning microscopy after incubation with cells. Briefly, HeLa cells were seeded at a density of 4×10^4 cells per well and mMSCs at 8×10^4 cells per well over sterile glass covers in 24 multiwell plates and incubated for 24 h at 37 °C. Then, the medium was replaced with 500 μL of the corresponding dendriplexes in SFM at an N/P ratio of 500, with 0.5 μg of pGFP per well. After 4 h of incubation at 37 °C, the cells were washed three times with PBS, fixed with 4% (v/v) paraformaldehyde and washed twice with PBS. Cell permeabilisation was accomplished with a PBS plus 1% BSA and 0.1% saponin solution and then actin filament staining was performed by incubating for 1 h in the dark with phalloidin-Alexa Fluor 488 diluted in the permeabilisation solution (1 : 200). Furthermore, washing steps were performed and then the nuclei were stained at the same time as the slides were mounted with a solution of DAPI in Fluoromount-G mounting medium (1 : 250). The samples were allowed to dry in the dark and sealed for later microscopic observation using a confocal Zeiss LSM 880 with the 63× oil immersion objective. DAPI fluorescence was observed at λ_{exc}: 405 nm and λ_{em}: 453 nm and Alexa Fluor at λ_{exc}: 488 nm and λ_{em}: 526 nm and finally, the rhodamine of the labelled DHPs was examined under λ_{exc}: 561 nm and λ_{em}: 635 nm. The Zen Blue 2.3 software and Image J were employed for image analysis.

Statistical analysis

The results are reported as mean ± SD (standard deviation) and the data were analysed by one-way analysis of variance (ANOVA) with Tukey *post-hoc* testing using the GraphPad Prism 8.0.2 software. $p < 0.05$, *; $p < 0.01$, **; $p < 0.001$, *** and $p < 0.0001$, **** were considered statistically significant.

Results and discussion

DHP synthesis

The synthesis strategy to obtain the final DHPs was done following our previous report[14] (schematically shown in Scheme S1, ESI†). It consists of the convergent attachment of the corresponding dendron N_3-[MPA,G2]-$(NHBoc)_4$ or N_3-[GMPA,G2]-$(NHBoc)_4$ to a MPA hyperbranched core of the second, third or fourth generation. Increasing the core generation while maintaining the dendron generation was thought as a feasible strategy to raise the number of the desired amino-terminal groups and avoid arduous synthetic steps. Previously, the commercial hyperbranched polyesters of the different generations (G2, G3 or G4) were functionalised with 4-pentynoic acid by means of Steglich esterification to introduce alkyne groups in the surroundings of the structures (see the ESI, section S1,† procedure I). These functional groups were essential to accomplish subsequent convergent coupling through the azide focal groups of the corresponding dendron by means of the CuAAC reaction (see the ESI, section S1,† procedure II). Finally, the *t*-Boc protecting groups were removed under acidic conditions with a mixture of $CHCl_3$: TFA (see the ESI, section S1,† procedure III) to obtain the amino-terminated DHPs as white solids.

DHP characterisation

The products were characterised by ^{1}H NMR, ^{13}C NMR, and FTIR spectroscopy and SEC. DHP(G2)-MPA and its corresponding precursors, the *t*-Boc protected DHP(G2)-MPA (NHBoc) and the alkyne functionalised hyperbranched core HP(G2)-≡, are shown here as representative examples to discuss the characterisation results.

NMR spectroscopical characterisation allowed us to confirm the correct product formation as well as to quantify the number of groups inserted. The Steglich alkyne addition was confirmed by the appearance of three ^{1}H NMR peaks at 2.55, 2.47 and 1.99 ppm, compared with the commercial HP, which correspond to the protons H-10′, H-11′ and H-13′, respectively (Fig. 2a). Moreover, their integration with respect to the unaltered methyl group in the bis-MPA core (H-7′) at 1.24 ppm revealed that 15, 31 or 62 alkyne groups were introduced for each HP generation (G2, G3 or G4), respectively. High levels of functionalisation were reached considering that the maximum theoretical ending groups are 16, 32 and 64 for each HP generation. The success of the CuAAC reaction could be observed by the appearance of a peak at 7.41 ppm that corresponds to the proton of the triazole ring, H-13, resulting from the cycloaddition (Fig. 2b). The appearance of two peaks at 146.1 ppm and 121.3 ppm in the ^{13}C NMR spectrum corresponding to the triazole carbons C-12 and C-13, respectively, also corroborate the progress of the reaction (see the ESI, Fig. S1†). The ^{1}H NMR spectrum also showed a chemical downfield shift of the protons adjacent to the alkyne groups as well as the inversion of their signals (Fig. 2b). Namely, the H-10′ and H-11′ peaks moved from 2.55 and 2.47 ppm to H-11 at 2.98 ppm and H-10 at 2.72 ppm when coupled to the dendrons. The integration of these downfield methylene signals (H-10 and H-11) and their comparison to the remaining non-functionalised ones (H-10′and H-11′), if any, allowed us to determine the number of dendrons covalently linked by the CuAAC reaction. According to this characterisation, the *t*-Boc-protected DHPs were estimated to bear a total number of terminal amino groups as follows: the bis-MPA series (DHP(G2)-MPA(NHBoc), DHP(G3)-MPA(NHBoc) and DHP(G4)-MPA (NHBoc)) contained 60, 124 and 248 dendrons, respectively, whereas the bis-GMPA series (DHP(G2)-GMPA(NHBoc), DHP (G3)-GMPA(NHBoc) and DHP(G4)-GMPA(NHBoc)) respectively included 60, 116 and 232 dendrons. Consequently, high levels of dendron attachments were obtained for both series (estimated as 100% for the bis-MPA and higher than 94% for the bis-GMPA series) and the expected polycationic DHPs for gene therapy were obtained.

In the FTIR spectra of DHP(G2)-MPA(NHBoc), a band at 3375 cm^{-1} corresponding to the N–H bond stretching appeared and the two almost overlapped intense bands around 1700 cm^{-1} (1731 and 1710) were due to the C═O bonds of the ester groups and the carbamate groups, respectively (Fig. 2c). In addition, the bands corresponding to the stretching of the ≡C–H and C≡C bonds of the HP(G2)-≡ (3281 and 2145, respectively) and the band at 2100 cm^{-1} corresponding to the azide group of the dendron were no longer observed, thus indicating the correct coupling to the dendrons.

SEC analysis revealed the absence of any remaining free reactive dendrons as well as low polydispersity values for all the *t*-Boc protected DHPs, ranging from 1.12 to 1.23. The retention times of the resulting DHPs underwent a considerable decrease compared with the hyperbranched cores without covalently added dendrons, as expected due to the increase in the Mw (see the ESI, Fig. S2†).

The final cleavage of the *t*-Boc groups to yield the amino terminated DHPs was assessed by the evolution of some signals in the NMR and FTIR spectra. On the one hand, the peak at 1.43 ppm in ^{1}H NMR and those at 156.0, 80.0 and 28.4 ppm in ^{13}C NMR, corresponding to the *t*-Boc groups disappeared in these spectra (see the ESI, Fig. S3a and b†). In return, two quadruplets centered at 163.0 and 118.2 ppm appeared corresponding to the carbons in the trifluoroacetate counterion (TFA^-) resulting from the deprotection method employed. This presence was also corroborated by the ^{19}F NMR spectra (see the ESI, Fig. S3c†). Regarding the FTIR spectra, the deprotection implied the disappearance of the NC═O st band at 1710 cm^{-1}, while the N–H st band around 3000 cm^{-1} got wider and more intense because of the terminal amine protonation and a new band due to the bending of the $N–H^+$ band that appeared around 1650 cm^{-1} (Fig. 2c).

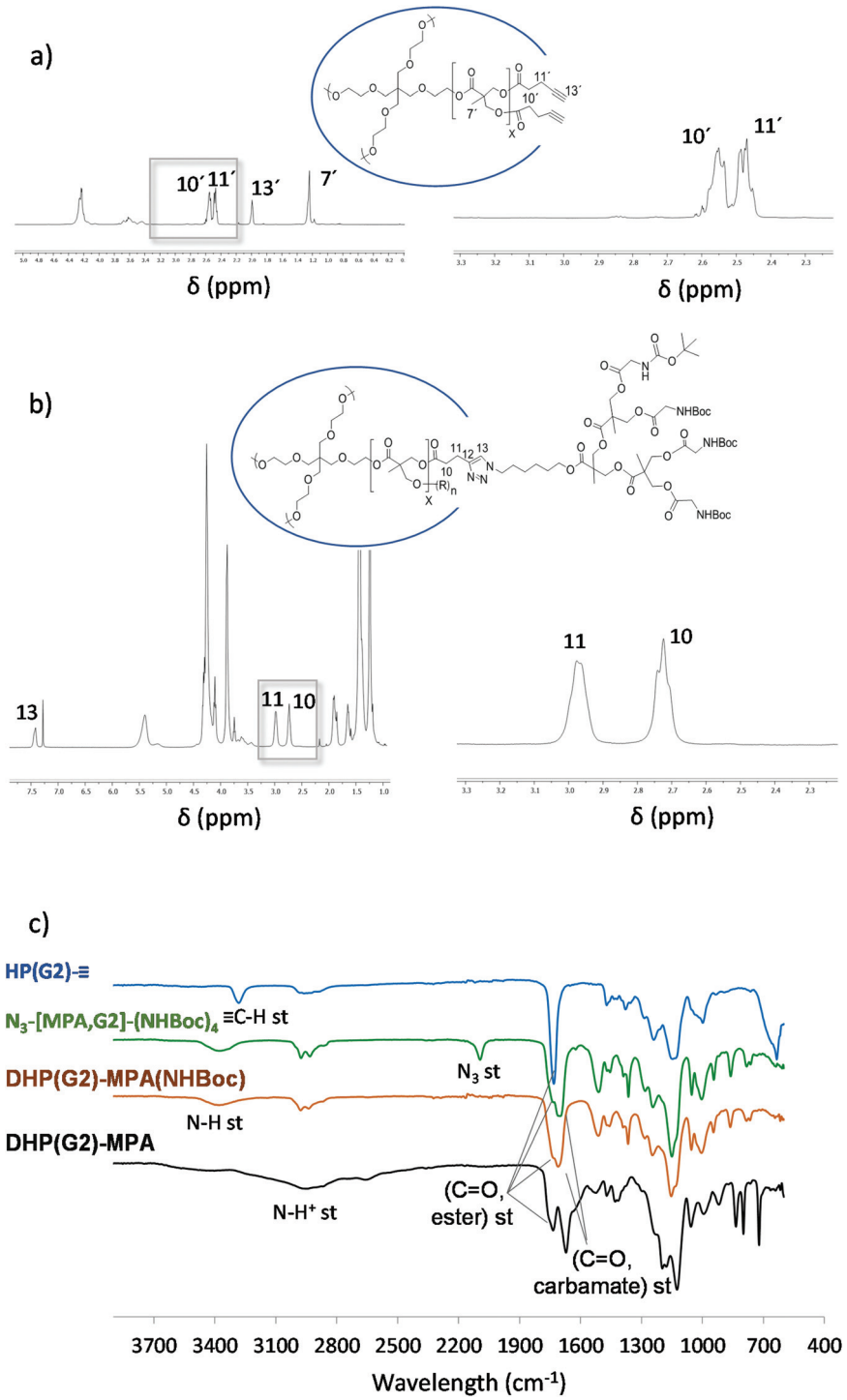

Fig. 2 Chemical structures and shifts in the ^{1}H NMR spectra of (a) HP(G2)-≡ and (b) DHP(G2)-MPA(NHBoc) ($CDCl_3$, 400 MHz). Full spectra are represented in the left side, while enlargements from 3.3 to 2.3 ppm corresponding to the spectra section indicated within the boxes are represented in the right side. (c) Compilation of FTIR spectra in the transmission mode of HP(G2)-≡ core (blue), N_3-[MPA,G2]-$(NHBoc)_4$ dendron (green), DHP(G2)-MPA(NHBoc) (orange) and deprotected DHP(G2)-MPA (black).

DHPs morphology in water

The synthesised DHPs showed complete solubilisation in water and their morphology was studied by TEM. The spherical objects observed and their size ranging from 10 to 20 nm suggest that the DHPs arrange in unimolecular micelles when dissolved in water (Fig. 3). This unimolecular arrangement has been previously reported for similar hyperbranched polymers

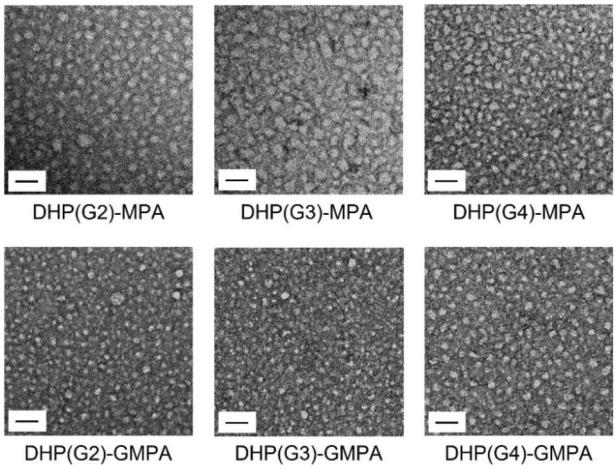

Fig. 3 Transmission electron microscopy (TEM) images of the DHPs in distilled water at 1 mg mL^{-1}. Scale bars: 50 nm.

based on a core–shell structure.[26] In addition, more compact unimolecular morphologies were observed for the bis-GMPA series when compared with the bis-MPA derivatives, which may be caused by the presence of intramolecular interactions favoured by the amide groups of the bis-GMPA dendrons. These observations were corroborated by the DLS measurement of the hydrodynamic diameter (D_H) of the aggregates in water. D_H data analysed in intensity and number are gathered in Table 1, and it can be observed that the sizes observed by TEM correlate with the DLS in number, as it has been previously described,[27] while DLS in intensity yields bigger sizes.[28,29] In addition, the small discrepancies observed by TEM and DLS (in number) may arise from the differences in the sample preparation for measurements. While DLS measures the sizes of the samples in solution, TEM imaging requires the drying and staining of the samples onto a grid. In addition, the ζ potential of the DHPs was measured (Table 2), which showed a positive surface charge in all the cases. No relevant differences were found in the surface charge among the DHP within the same series, being around 6.3 for the bis-MPA series and around 4.5 for the bis-GMPA DHPs. The differences upon comparing both series of DHPs could be related to the interactions of the terminal amino groups with the inner amide groups of the bis-GMPA dendrons that lead to a lesser number of positive charges exposed on the surface and then a decrease in their ζ potential.

Table 2 ζ potential of empty DHPs and their dendriplexes with pGFP (N/P ratios 25 and 500) and siGFP (N/P ratios 150 and 750). Results are expressed as the average in mV

DHPs	Empty carriers	pGFP dendriplexes N/P 25	pGFP dendriplexes N/P 500	siGFP dendriplexes N/P 150	siGFP dendriplexes N/P 750
DHP(G2)-MPA	6.8	3.7	6.5	8.1	12.1
DHP(G3)-MPA	5.9	4.6	12.3	12.8	13.5
DHP(G4)-MPA	6.1	5.5	13.1	11.2	10.6
DHP(G2)-GMPA	4.5	3.6	3.6	6.4	5.0
DHP(G3)-GMPA	4.3	2.5	8.5	9.3	6.0
DHP(G4)-GMPA	4.7	0.6	4.1	7.0	7.4

Dendriplexes formation and characterisation

The gel retardation assay allowed us to identify the minimum N/P ratios at which the nucleic acids were totally complexed by the DHPs. The commercial transfection reagents Lipofectamine 3000 (lipidic formulation) and SuperFect (dendritic formulation) were used under supplier specifications and their w/w ratios for nucleic acid complexation were determined by following the same procedure. As seen in Fig. 4a, pGFP was totally complexed at a N/P ratio of 25 by all the DHPs studied, when no band of free pGFP was observed, although partial complexation could be observed at lower ratios, especially for the highest DHP generation. Even though the majority of the siGFP was complexed by the DHPs at a N/P ratio of 100, especially for G4-DHPs, the N/P complexation

Table 1 Hydrodynamic diameters (D_H) of empty DHPs and their dendriplexes with pGFP (N/P ratios of 25 and 500) and siGFP (N/P ratios 150 and 750). D_H were measured after number or intensity treatment. Data are given as mean ± SD (in nm) and the percentage of each population is included in brackets if applicable

DHPs	Empty carriers D_H number	pGFP dendriplexes N/P 25 D_H intensity	pGFP dendriplexes N/P 500	siGFP dendriplexes N/P 150	siGFP dendriplexes N/P 750
DHP(G2)-MPA	12 ± 3	197 ± 8 (91) 32 ± 4 (9)	349 ± 15 (92) 12 ± 2 (8)	236 ± 15	164 ± 6
DHP(G3)-MPA	15 ± 4	210 ± 18 (92) 29 ± 3 (8)	251 ± 5 (100)	269 ± 7	224 ± 16
DHP(G4)-MPA	18 ± 1	166 ± 19 (85) 29 ± 8 (15)	271 ± 18 (72) 22 ± 3 (28)	259 ± 14	165 ± 10
DHP(G2)-GMPA	7 ± 1	183 ± 18 (89) 34 ± 12 (11)	248 ± 12 (82) 4 ± 1 (18)	253 ± 15	184 ± 7
DHP(G3)-GMPA	14 ± 2	190 ± 40 (69) 42 ± 6 (31)	371 ± 14 (85) 43 ± 5 (15)	234 ± 13	171 ± 4
DHP(G4)-GMPA	9 ± 2	128 ± 1 (88) 19 ± 2 (12)	243 ± 9 (78) 15 ± 1 (22)	251 ± 9	276 ± 15

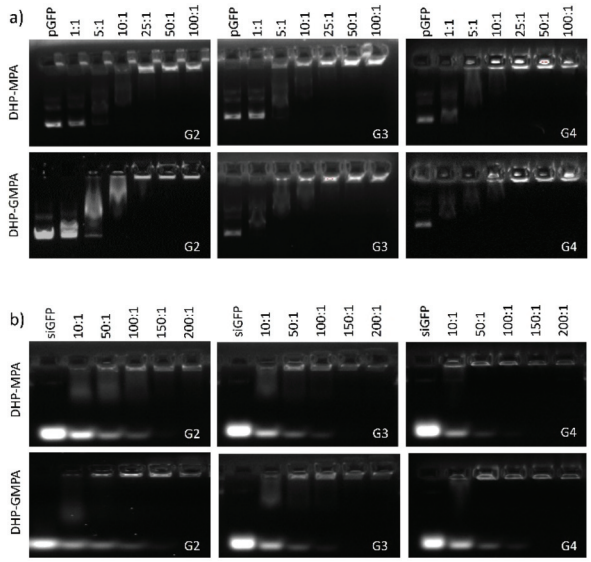

Fig. 4 Complex formation between polycationic carriers and nucleic acids. (a) Gel retardation of pGFP in the presence of increasing amounts of DHP and (b) Gel retardation of siGFP in the presence of increasing amounts of DHP.

ratio for further cell studies was established at 150 in all the cases to ensure whole nucleic acid capture (Fig. 4b).

The complexation involving the commercial reagents also needed more amount of polycationic DHP in the case of siGFP (w/w ratio 7 for Lipofectamine and 3 for SuperFect) than pGFP (w/w ratios 1.5 and 2 for Lipofectamine and SuperFect, respectively) (see the ESI, Fig. S5†). These prominent differences between the nucleic acid complexation ratios may reside in the size and rigidity of each construct.[30,31] Considering that all DHPs have a similar number of N^+ per mass unit (between 1.5 $\times 10^{18}$ and 1.8 $\times 10^{18}$ N^+ mg^{-1}), differences in the total number of peripheral amino groups have shown not to have a strong influence on the N/P ratio of dendriplex formation for the range of DHP generations studied. Besides, the presence of inner amide groups in the series of DHPs containing the bis-GMPA dendron (DHP(G2)-GMPA, DHP(G3)-GMPA and DHP (G4)-GMPA) does not affect the amount of DHPs required to form the complexes compared to the bis-MPA DHP series (DHP(G2)-MPA, DHP(G3)-MPA and DHP(G4)-MPA). A slight difference is only observed for DHP(G3), since DHP(G3)-GMPA starts the pGFP complexation at the N/P ratio of 1 whereas its bis-MPA homologue needs to increase the N/P ratio to 5 to modify the electrophoretic mobility of the nucleic acid.

The morphological characterisation of the dendriplexes at different N/P ratios was carried out together with the characterisation of the empty DHPs in order to elucidate the nucleic acid influence on the established structures. Different techniques were used for their characterisation: dynamic light scattering (DLS), ζ potential, atomic force microscopy (AFM) and cryo-TEM.

The sizes determined by DLS in intensity (see Table 1) showed two size populations of nanoparticles for the majority of dendriplexes involving pGFP, while only one population was observed for the siGFP dendriplexes. This may be related to the higher flexibility exhibited by the plasmid DNA that allows more possibilities of conformation. The bigger population of dendriplexes with pGFP at the forming ratio (N/P 25) displayed sizes below 210 nm that predominated in abundance over the smaller population (around 30 nm), but it is important to consider that DLS in intensity tends to overestimate the particles size in detriment to the smaller ones.[28,29] These diameters were incremented when the ratio N/P was raised to 500. siGFP dendriplexes underwent less size variations once the complexes were already formed, observing diameters around 250 nm for all dendriplexes at the N/P ratio of 150 and more compact structures around 200 nm at the highest ratio assayed (N/P 750).

The measurement of the ζ potential (see Table 2) revealed that all the dendriplexes presented a positive surface charge, thus indicating that the nucleic acid had been completely complexed, as was evidenced by the gel retardation assays (see Fig. 4). Besides, a general increase in the charge was observed when increasing the N/P ratio due to the presence of a higher number of molecules of the positively charged DHPs. Regarding both DHP series, dendriplexes with DHP-GMPA vectors presented lower ζ potential values than those with the DHP-MPA of the same generation. This could be due to the location of the peripheral amino groups of the DHP in a more internal cavity of the complex and it may be related to interactions with the inner amide groups of the bis-GMPA dendrons.

As an example, the formation of dendriplexes between pGFP and the biggest DHP of the bis-MPA series, DHP(G4)-MPA, was further investigated by AFM and cryo-TEM (Fig. 5).

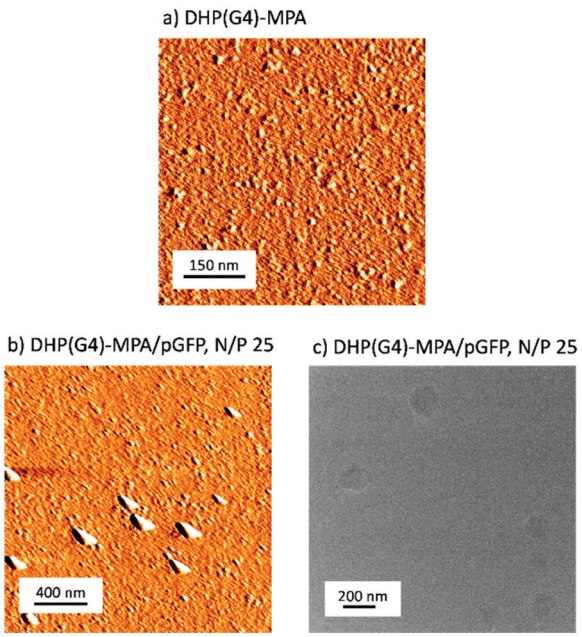

Fig. 5 AFM topographic images of DHP(G4)-MPA empty aggregates (a) and the dendriplexes formed with pGFP at a N/P ratio of 25 and (b) Cryo-TEM image of these dendriplexes (c).

As observed in DLS measurements, two size populations were found by AFM for the complexes involving pGFP. Namely, for the DHP(G4)-MPA/pGFP dendriplexes at a N/P ratio of 25, some large aggregates around 200 nm in length were found, while a more abundant population of small, rounded structures of *ca.* 20 nm were observed, probably corresponding to empty DHPs (Fig. 5b). The discrepancy between the abundance of populations observed between DLS and AFM can be related to the fact that the DLS data in intensity tend to overestimate the presence of the biggest population. However, the DLS in number reflects more accurately these AFM sizes, yielding D_H below 33 ± 2 nm for all the dendriplexes with pGFP (see the ESI, Table S2†). The sizes observed by cryo-TEM for DHP(G4)-MPA/pGFP dendriplexes at a N/P ratio of 25 were in the range of 150–200 nm (Fig. 5c), which is in agreement with the values obtained by DLS in intensity.

Transfection and viability experiments

***In vitro* pGFP transfection.** After an initial optimisation of the experimental conditions regarding incubation time and the amount of loaded pGFP (see the ESI, Fig. S6†), 4 h of incubation and 0.2 μg of pGFP were established as the most appropriate parameters to carry on the comparative study of transfection ability on our DHPs.

The ability of all the DHPs as gene delivery vectors for pGFP in a broad range of N/P ratios was evaluated in two different cell lines: HeLa and the mesenchymal cells mMSCs (the whole data are gathered in the ESI, Fig. S7† and the ratios in w : w in Table S3†). It can be observed that the naked pGFP did not have any transfection ability by itself under these conditions, corroborating the necessity to employ a vector to facilitate its delivery into the cells. The trend in pGFP transfection efficiency exerted by the N/P ratios follows the same tendency within the two cell lines (Fig. S7†), with better values observed for the highest N/P ratio assessed, namely N/P = 500. In order to evaluate the effect of the type of DHP (bis-GMPA or bis-MPA) and generation (G2, G3, and G4) in pGFP transfection and viability results in both cell lines, the results at the ratio of N/P 500 are gathered in Fig. 6.

Upon comparing the two DHP series (bis-MPA and bis-GMPA), it is remarkable to see the absence of any transfection activity in either of the cell lines with those DHPs including the bis-GMPA dendron (DHP(G2)-GMPA, DHP(G3)-GMPA and DHP(G4)-GMPA). Although, according to the gel retardation assay (see Fig. 4), the dendriplexes were all successfully formed at the N/P ratio of 25 and their final transfection activity showed significant differences (see Fig. 6). Indeed, the data seem to suggest that the presence of the bis-GMPA dendrons somehow hinders the final expression of the GFP protein as lower values (below 0.3 a.u.) are observed in all the cases comprising DHPs-GMPA (see Fig. 6).

The DHPs of the bis-MPA series presented good characteristics as non-viral pGFP vectors. Indeed, they showed higher transfection efficiencies than SuperFect, a commercially available gene delivery vector with a dendritic structure. Besides, the results obtained for the DHPs in the mMSCs were even higher than that for the lipid based Lipofectamine 3000 control. In this line, larger transfection efficiencies were

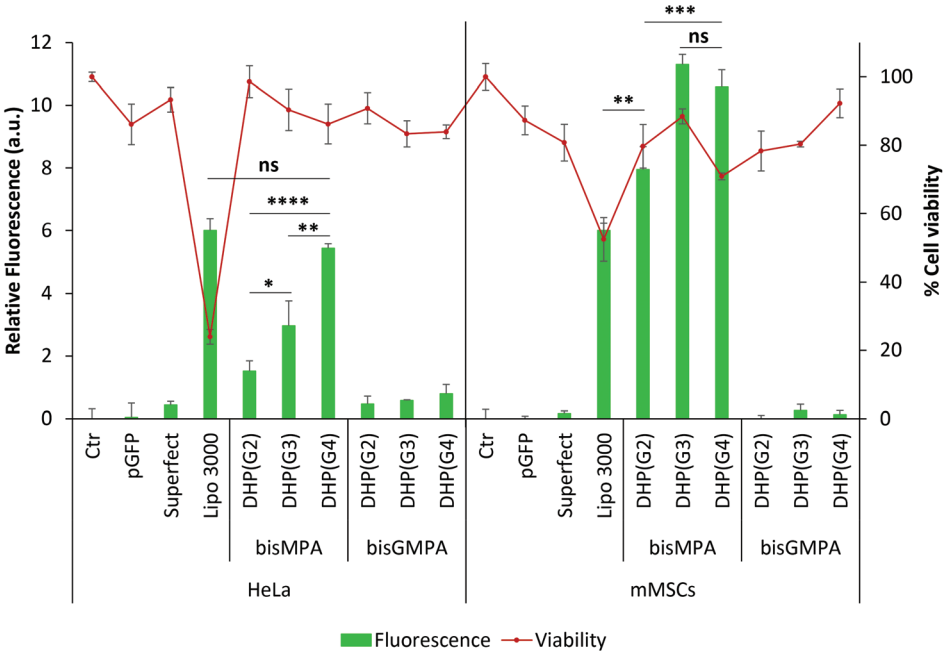

Fig. 6 Transfection experiments with pGFP in HeLa (left) and mMSC (right) cell lines. All the DHPs of the bis-MPA and bis-GMPA series were assayed as vectors at the N/P ratio of 500. Controls without treatment, naked pGFP, with SuperFect and with Lipofectamine 3000 are also included for each cell lines. Green bars show the transfection efficiency and red points indicate cell viability. Error bars indicate the standard deviation (SD) (n = 3). Statistical analysis was performed by one-way ANOVA; ns, $p > 0.05$; *, $p < 0.05$; **, $p < 0.01$; ***, $p < 0.001$; and ****, $p < 0.0001$.

observed when the N/P ratio was significantly higher than that established as the minimum for dendriplex formation, which had been previously observed by us.[14] Among the bis-MPA series, the bigger the polyester core generation, the more activity it exhibited as a pGFP vector. At the N/P ratio of 500, even the small DHP(G2)-MPA showed better transfection efficiency than the commercial lipidic Lipofectamine 3000 (8.0 a.u. *versus* 6.0 a.u.). It is interesting to note that no significant differences in the levels of transfection were found at the N/P ratio of 500 for DHP(G3)-MPA and DHP(G4)-MPA (11.3 a.u. and 10.6 a.u., respectively). The ζ potential values of these two dendriplexes formed between DHP(G3)-MPA or DHP(G4)-MPA with pGFP at the N/P ratio of 500 are the highest ones among the pGFP complexes (12.3 and 13.1 mV, respectively, see Table 2), which may contribute to a more favourable cellular uptake, thus benefiting subsequent transfection activity. The low cytotoxicity of these dendritic vectors, with above 70% viability in all the cases, arose as another advantageous feature compared to the Lipofectamine vector.

Fluorescence microscopy was used to corroborate the spectroscopic results. As a representative example, the fluorescence on mMSCs after transfection with DHP(G4)-MPA and pGFP at different N/P ratios is shown in Fig. 7. The expression of green fluorescence was observed to increase upon increasing the N/P ratio from 100 to 500. While scarce fluorescence was observed at the N/P of 100, at the highest ratio assayed, N/P 500, the levels of GFP expression were higher than those of the cells transfected with the commercial Lipofectamine 3000. These qualitative results are in good agreement with the previous spectroscopic data measured (see Fig. 6 and S7†).

In general terms, better pGFP transfection results were obtained within the mMSCs. Interestingly, all DHPs of the bis-MPA series show superior values for pGFP transfection compared to previous bis-MPA DHPs reported by us.[14] Whereas the current series contains bis-MPA dendrons of generation 2 and were used at a N/P ratio of 500 for better transfection, previously reported series were prepared with bis-MPA dendrons of generation 3 at a maximum N/P ratio of 200. Thus, for these materials, larger transfection values can be obtained by increasing the N/P ratio even if a lower amount of ammonium groups are present at the surface.

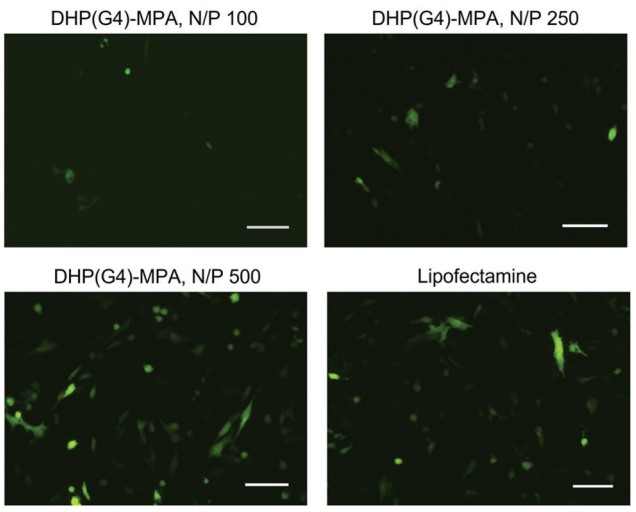

Fig. 7 Fluorescence images of mMSC cells expressing GFP after incubation with the plasmid in combination with DHP(G4)-MPA at N/P ratios 100, 250 or 500 and the plasmid with Lipofectamine 3000 as control. Scale bars: 100 μm.

***In vitro* siGFP transfection.** The DHPs showed similar trends for the transfection of siGFP in the two cell lines, HeLa-GFP and mMSCs-GFP, at a broad range of N/P ratios tested (the whole data are gathered in the ESI, Fig. S8† and the ratios in w : w in Table S4†). As for the pGFP transfection section (see Fig. 6), the results at the highest N/P ratio, *i.e.* 750, are shown in Fig. 8. Among the DHPs, the bis-MPA derivatives showed better transfection activity than their GMPA counterparts. Focussing on the DHP-MPA series, a core generation dependence was observed again, being the levels of DHP(G4)-MPA fluorescence inhibition at a N/P ratio of 750 (35%) comparable to those of Lipofectamine (34%). An improvement in the transfection efficiency was observed upon increasing the N/P ratio but it compromised the cell viability levels (see the ESI, Fig. S8†). The dendriplex formulation that yielded the higher rate of fluorescence inhibition, DHP(G4)-MPA at a N/P ratio of 750, was also responsible for a 60% decay in cell viability. No relevant differences were found in the activity of DHP(G2)-MPA and DHP (G3)-MPA as siGFP vectors (20 and 19% of fluorescence inhibition, respectively) but the differences in cell viability postulate DHP(G3)-MPA as a better vector at a N/P ratio of 750.

The levels of green fluorescence expression were also assessed by fluorescence microscopy. Apart from Lipofectamine 3000-transfected cells, control of the wild-type mMSCs-GFP cells was included to visualise the highest level of fluorescence reached within this cell line. As a representative example, images of transfection with DHP(G4)-MPA and siGFP at different N/P ratios (300, 500 and 750) are shown (Fig. 9). As previously observed in the spectroscopic fluorescence determination (see Fig. S8†), the increase in the N/P ratio from 300 to 750 resulted in a decrease in fluorescence levels, that is, an improvement in the siGFP silencing activity. The largest GFP expression inhibition in mMSCs-GFP with a DHP vector was reached after transfection with DHP(G4)-MPA/siGFP at a N/P ratio of 750, whose levels of fluorescence were comparable to those of the mMSCs-GFP cells transfected with Lipofectamine 3000.

Internalisation and cellular distribution

The most promising DHP combinations with pGFP were evaluated in terms of cell internalisation and intracellular distribution of both cell lines, HeLa and mMSCs. Dendriplexes between DHP(G4)-MPA and DHP(G4)-GMPA at a N/P ratio of 500 were chosen to carry out this assay. To visualise the dendriplexes within the intracellular compartments by confocal microscopy, the DHPs were previously labelled with the fluorophore rhodamine B (as explained in the ESI, section S2†). The results are shown in Fig. 10.

The internalisation of the dendriplexes containing DHP (G4)-MPA-RhB or DHP(G4)-GMPA-RhB was low in both cell

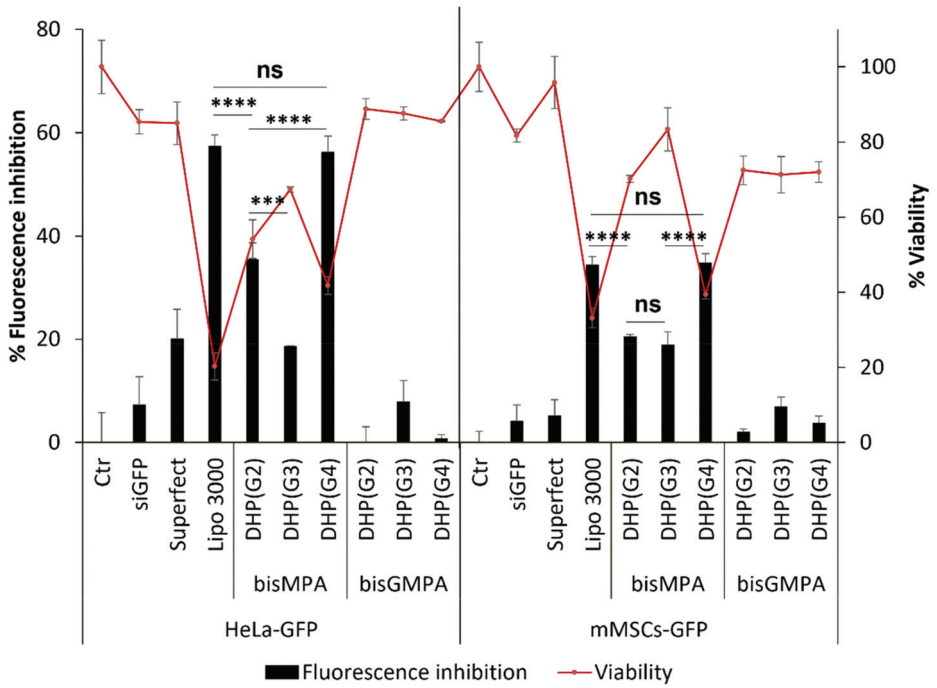

Fig. 8 Transfection experiments with siGFP in HeLa-GFP (left) and mMSC-GFP (right) cell lines. All the DHPs of the bis-MPA and bis-GMPA series were assayed as vectors at the N/P ratio of 750. Controls without treatment, naked siGFP, with Superfect and with Lipofectamine 3000 are also included for each cell lines. Black bars show transfection efficiency and red points indicate cell viability. Error bars indicate the standard deviation (SD) (n = 3). Statistical analysis was performed by one-way ANOVA; ns, $p > 0.05$; **, $p < 0.01$; ***, $p < 0.001$.

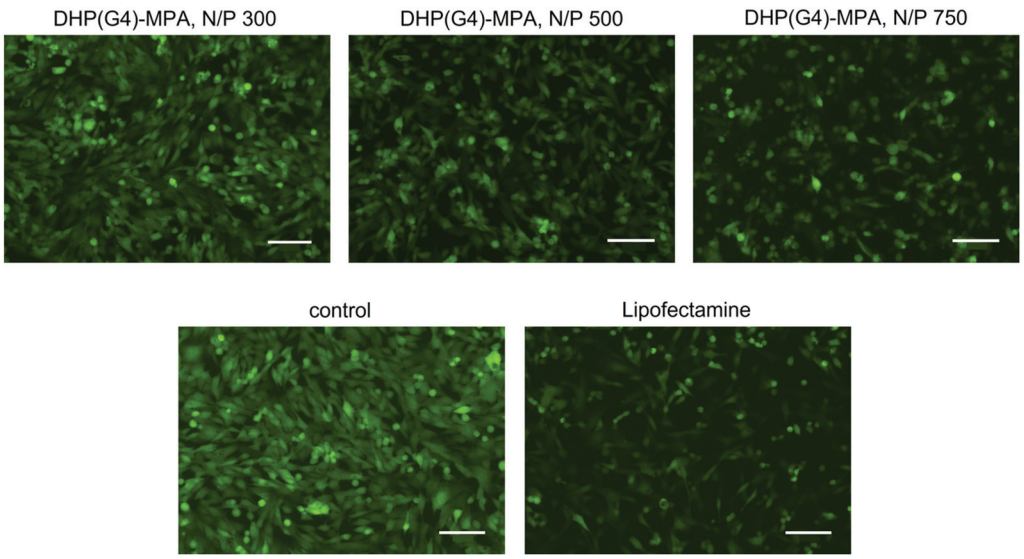

Fig. 9 Fluorescence images of mMSCs-GFP cells showing a reduction in the GFP expression after incubation with the siGFP in combination with DHP(G4)-MPA at N/P ratios 300, 500 or 750. siGFP with Lipofectamine 3000 and the wild type cells are included as controls. Scale bars: 100 μm.

lines. Interestingly, few dendriplexes composed of DHP(G4)-MPA-RhB were found within the HeLa cell line (Fig. 10a, top row) whereas the confocal microscopy did not show any DHP (G4)-GMPA-RhB dendriplexes inside these cells (Fig. 10a, the bottom row). In the case of mMSCs, a higher number of dendriplexes containing DHP(G4)-MPA-RhB were found inside the cells (Fig. 10b, top row), while just few DHP(G4)-GMPA-RhB dendriplexes were found on the cellular surface (Fig. 10b, bottom row). Moreover, the location of the DHP(G4)-MPA-RhB dendriplexes revealed their distribution along the cellular morphology, with the presence of some aggregates colocalising with actin in the peripheral cytoplasm and others in the surroundings of the cellular nucleus. The absence of DHP(G4)-GMPA-RhB dendriplexes inside the HeLa cells and their scarce

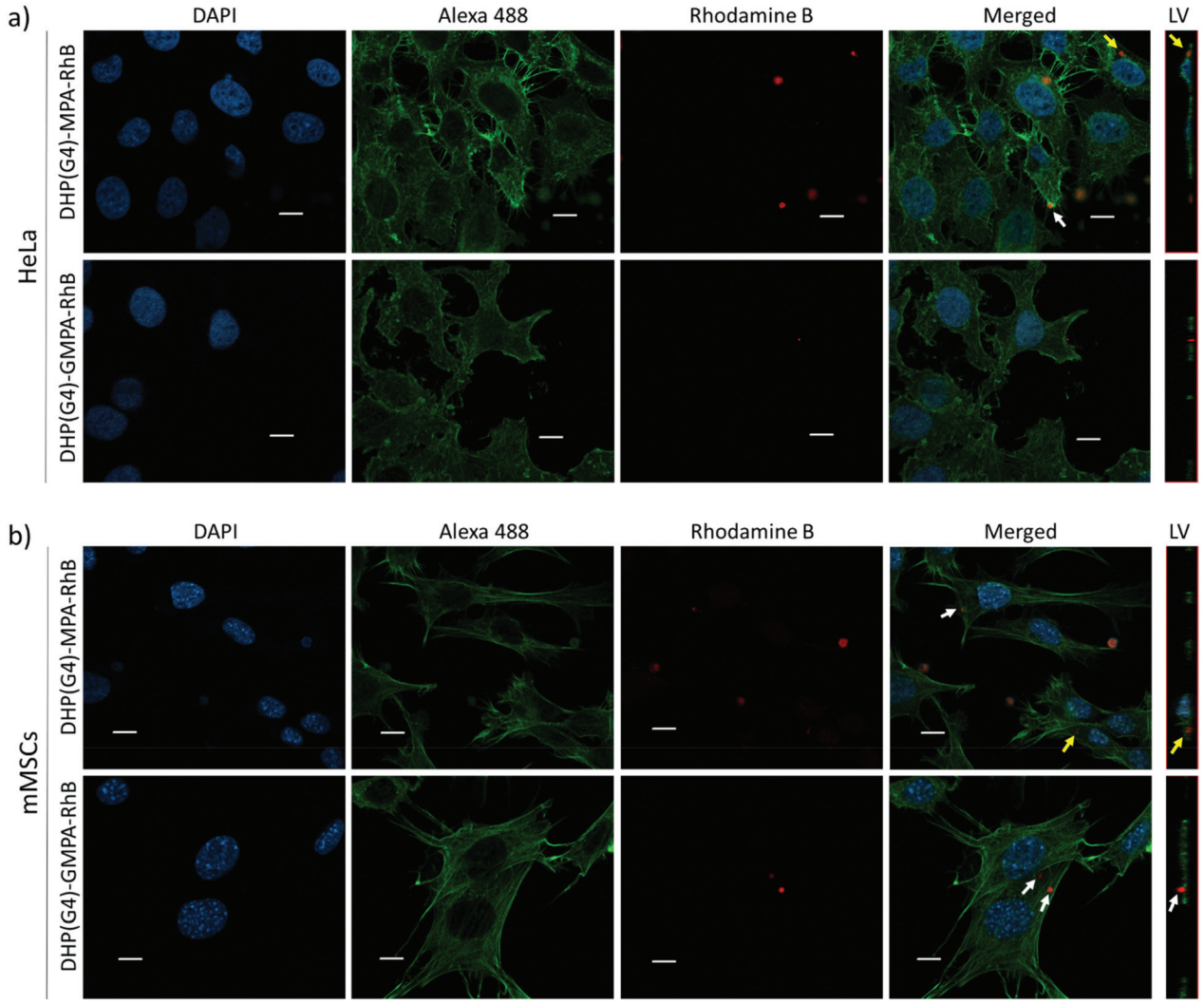

Fig. 10 Confocal *z*-stack projections of the internalisation dendriplexes DHP(G4)-MPA-RhB and DHP(G4)-GMPA-RhB with pGFP at an N/P ratio of 500 in (a) HeLa and (b) mMSCs. Scale bars: 10 μm. Color code: blue, nuclei; green, actin; and red, rhodamine B. Single images for each channel are represented as well as all channels merged and some representative lateral views (LV). White arrows indicate dendriplexes inside the cells or on the surface and yellow arrows indicate dendriplexes near the nucleus.

presence only at the surface of the mMSCs is in good agreement with the low transfection efficiencies previously measured (see Fig. 6). A plausible explanation could be related to the lower ζ potential values observed for DHPs-GMPA compared to DHPs-MPA (see Table 2), which could reduce their cellular uptake.[32] In addition, the establishment of hydrogen bonds between the bis-GMPA dendrons present in the DHP could contribute to the better entrapment of pGFP of the dendriplex, thus hampering subsequent release.[33,34]

Conclusions

A series of hyperbranched dendronized polymers (DHP) of G2, G3 and G4 with dendrons built either with bis-MPA or bis-GMPA have been synthesised and their ability to complex plasmid DNA and siGFP have been demonstrated. Their transfection activity as non-viral vectors has revealed better suitability in terms of the functionality of the DHP-MPA derivatives over their DHP-GMPA homologues and, more remarkably, over other highly efficient commercial dendritic-based reagents. Most interestingly, transfection levels as good as the lipidic commercial Lipofectamine 3000 were obtained for siGFP transfection with DHP(G4)-MPA at a N/P ratio of 750 and almost a 2-fold improvement in the pGFP transfection efficiency of Lipofectamine 3000 was achieved with DHP(G3)-MPA and DHP(G4)-MPA at a N/P ratio of 500. A generation dependence and the influence of some parameters like N/P ratios or incubation times on the transfection efficiency were observed. The lower efficiency obtained for the DHP-GMPA series as gene delivery vectors compared to the DHP-MPA series is proposed to occur mainly by the lower ζ potential values of the former, which limit their cellular internalisation. In addition, the establishment of hydrogen bonds between the

bis-GMPA dendrons may produce a better entrapment of the nucleic acids and consequently hamper their release. Finally, the good results obtained in gene delivery with the mesenchymal cell line, especially for pGFP transfection, are quite relevant, as this type of cells are usually difficult to transfect,[35] thus opening a promising landscape for gene delivery into these pluripotent cells with a wide range of further applications.

Author contributions

The manuscript was written through the contribution of all authors. All authors have given approval to the final version of the manuscript.

Conflicts of interest

There are no conflicts to declare.

Acknowledgements

This research was supported by the Ministerio de Ciencia, Innovación y Universidades, Spain (PGC2018-097583-B-I00) and funds for the Research Group E47_20R by Gobierno de Aragon-FSE. MSA thanks the Ministerio de Ciencia, Innovación y Universidades, for her grant (BES-2016-078774). The authors would like to acknoweledge the Laboratorio de Microscopia Avanzada-LMA (Instituto de Nanociencia y Materiales de Aragón-Universidad de Zaragoza), Servicio General de Apoyo a la Investigación-SAI (Universidad de Zaragoza) and Servicios Cientifico-Técnicos of CEQMA (CSIC-Universidad de Zaragoza) and of CIBA (IACS-Universidad de Zaragoza) for their support. The authors would also like to thank for the collaboration of Juan Calvet Seral for his help with plasmid amplification and Dr Pilar Martín-Duque for the supply of cells and the advice on cell culturing and general discussion.

References

1 S. Razi Soofiyani, B. Baradaran, F. Lotfipour, T. Kazemi and L. Mohammadnejad, Gene Therapy, Early Promises, Subsequent Problems, and Recent Breakthroughs, *Adv. Pharm. Bull.*, 2013, **3**(2), 249–255, DOI: **10.5681/apb.2013.041**.

2 I. Lostalé-Seijo and J. Montenegro, Synthetic Materials at the Forefront of Gene Delivery, *Nat. Rev. Chem.*, 2018, **2**(10), 258–277, DOI: **10.1038/s41570-018-0039-1**.

3 A. Nyamay'Antu, M. Dumont, V. Kedinger and P. Erbacher, Non-Viral Vector Mediated Gene Delivery: The Outsider to Watch Out For in Gene Therapy, *Cell Gene Ther. Insights*, 2019, **5**(S1), 51–57, DOI: **10.18609/cgti.2019.007**.

4 K. Lundstrom, Viral Vectors in Gene Therapy, *Diseases*, 2018, **6**(2), 42, DOI: **10.3390/diseases6020042**.

5 J. T. Bulcha, Y. Wang, H. Ma, P. W. L. Tai and G. Gao, Viral Vector Platforms within the Gene Therapy Landscape, *Signal Transduction Targeted Ther.*, 2021, **6**(1), 53, DOI: **10.1038/s41392-021-00487-6**.

6 J. L. Shirley, Y. P. de Jong, C. Terhorst and R. W. Herzog, Immune Responses to Viral Gene Therapy Vectors, *Mol. Ther.*, 2020, **28**(3), 709–722, DOI: **10.1016/j.ymthe.2020.01.001**.

7 M. Ramamoorth and A. Narvekar, Non Viral Vectors in Gene Therapy- An Overview, *J. Clin. Diagn. Res.*, 2015, **9**(1), GE01–GE06, DOI: **10.7860/JCDR/2015/10443.5394**.

8 Y. Sung and S. Kim, Recent Advances in the Development of Gene Delivery Systems, *Biomater. Res.*, 2019, **23**(1), 8, DOI: **10.1186/s40824-019-0156-z**.

9 S. Patil, Y.-G. Gao, X. Lin, Y. Li, K. Dang, Y. Tian, W.-J. Zhang, S.-F. Jiang, A. Qadir and A.-R. Qian, The Development of Functional Non-Viral Vectors for Gene Delivery, *Int. J. Mol. Sci.*, 2019, **20**(21), 5491, DOI: **10.3390/ijms20215491**.

10 J. Yang, Q. Zhang, H. Chang and Y. Cheng, Surface-Engineered Dendrimers in Gene Delivery, *Chem. Rev.*, 2015, **115**(11), 5274–5300, DOI: **10.1021/cr500542t**.

11 L. Palmerston Mendes, J. Pan and V. P. Torchilin, Dendrimers as Nanocarriers for Nucleic Acid and Drug Delivery in Cancer Therapy, *Molecules*, 2017, **22**(9), 1401, DOI: **10.3390/molecules22091401**.

12 H. Hu, H. Wang, S. Liang, X. Li and D. Wang, Synthesis and Characterization of a PAMAM Dendrimer Nanocarrier Functionalized by HA for Targeted Gene Delivery Systems and Evaluation in Vitro, *J. Biomater. Sci., Polym. Ed.*, 2020, 1–24, DOI: **10.1080/09205063.2020.1827921**.

13 P. Laskar, S. Somani, M. Mullin, R. J. Tate, M. Warzecha, D. Bowering, P. Keating, C. Irving, H. Y. Leung and C. Dufès, Octadecyl Chain-Bearing PEGylated Poly (Propyleneimine)-Based Dendrimersomes: Physicochemical Studies, Redox-Responsiveness, DNA Condensation, Cytotoxicity and Gene Delivery to Cancer Cells, *Biomater. Sci.*, 2021, **9**(4), 1431–1448, DOI: **10.1039/D0BM01441A**.

14 A. Lancelot, R. González-Pastor, A. Concellón, T. Sierra, P. Martín-Duque and J. L. Serrano, DNA Transfection to Mesenchymal Stem Cells Using a Novel Type of Pseudodendrimer Based on 2,2-Bis(Hydroxymethyl) Propionic Acid, *Bioconjugate Chem.*, 2017, **28**(4), 1135–1150, DOI: **10.1021/acs.bioconjchem.7b00037**.

15 A. Lancelot, R. González-Pastor, R. Clavería-Gimeno, P. Romero, O. Abian, P. Martín-Duque, J. L. Serrano and T. Sierra, Cationic Poly(Ester Amide) Dendrimers: Alluring Materials for Biomedical Applications, *J. Mater. Chem. B*, 2018, **6**(23), 3956–3968, DOI: **10.1039/C8TB00639C**.

16 M. J. Serramía, S. Álvarez, E. Fuentes-Paniagua, M. I. Clemente, J. Sánchez-Nieves, R. Gómez, J. de la Mata and M.Á Muñoz-Fernández, In Vivo Delivery of SiRNA to the Brain by Carbosilane Dendrimer, *J. Controlled Release*, 2015, **200**, 60–70, DOI: **10.1016/j.jconrel.2014.12.042**.

17 F. Saviano, T. Lovato, A. Russo, G. Russo, C. R. Bouton, R. J. Shattock, C. Alexander, F. Quaglia, A. K. Blakney, P. Gurnani and C. Conte, Ornithine-Derived Oligomers and Dendrimers for *in Vitro* Delivery of DNA and *Ex Vivo* Transfection of Skin Cells *via* SaRNA, *J. Mater. Chem. B*, 2020, **8**(22), 4940–4949, DOI: **10.1039/D0TB00942C**.

18 J. Zhou, S. Ma, Y. Zhang, Y. He, J. Yang, H. Zhang, K. Luo and Z. Gu, Tunable Membrane-Penetrating Bioreductive Nanogels Based on Guanidinylated Dendrimers for Programmable Gene Delivery, *Appl. Mater. Today*, 2020, **20**, 100646, DOI: **10.1016/j.apmt.2020.100646**.

19 A. Ihnatsyeu-Kachan, V. Dzmitruk, E. Apartsin, O. Krasheninina, M. Ionov, S. Loznikova, A. Venyaminova, K. Miłowska, D. Shcharbin, S. Mignani, M. A. Muñoz-Fernández, J.-P. Majoral and M. Bryszewska, Multi-Target Inhibition of Cancer Cell Growth by SiRNA Cocktails and 5-Fluorouracil Using Effective Piperidine-Terminated Phosphorus Dendrimers, *Colloids Interfaces*, 2017, **1**(1), 6, DOI: **10.3390/colloids1010006**.

20 Y. Wang, L. Li, N. Shao, Z. Hu, H. Chen, L. Xu, C. Wang, Y. Cheng and J. Xiao, Triazine-Modified Dendrimer for Efficient TRAIL Gene Therapy in Osteosarcoma, *Acta Biomater.*, 2015, **17**, 115–124, DOI: **10.1016/j.actbio.2015.01.007**.

21 A. Lederer, W. Burchard, T. Hartmann, J. S. Haataja, N. Houbenov, A. Janke, P. Friedel, R. Schweins and P. Lindner, Dendronized Hyperbranched Macromolecules: Soft Matter with a Novel Type of Segmental Distribution, *Angew. Chem., Int. Ed.*, 2015, **54**(43), 12578–12583, DOI: **10.1002/anie.201504059**.

22 E. M. Coma-Cros, A. Lancelot, M. San Anselmo, L. N. Borgheti-Cardoso, J. J. Valle-Delgado, J. L. Serrano, X. Fernàndez-Busquets and T. Sierra, Micelle Carriers Based on Dendritic Macromolecules Containing Bis-MPA and Glycine for Antimalarial Drug Delivery, *Biomater. Sci.*, 2019, **7**(4), 1661–1674, DOI: **10.1039/C8BM01600C**.

23 A. Andrzejewska, B. Lukomska and M. Janowski, Concise Review: Mesenchymal Stem Cells: From Roots to Boost, *Stem Cells*, 2019, **37**(7), 855–864, DOI: **10.1002/stem.3016**.

24 J. Movellan, P. Urbán, E. Moles, J. M. de la Fuente, T. Sierra, J. L. Serrano and X. Fernàndez-Busquets, Amphiphilic Dendritic Derivatives as Nanocarriers for the Targeted Delivery of Antimalarial Drugs, *Biomaterials*, 2014, **35**(27), 7940–7950, DOI: **10.1016/j.biomaterials.2014.05.061**.

25 I. Horcas, R. Fernández, J. M. Gómez-Rodríguez, J. Colchero, J. Gómez-Herrero and A. M. Baro, WSXM: A Software for Scanning Probe Microscopy and a Tool for Nanotechnology, *Rev. Sci. Instrum.*, 2007, **78**(1), 013705, DOI: **10.1063/1.2432410**.

26 P. Sun, N. Wang, X. Jin and X. Zhu, "Bottom-Up" Construction of Hyperbranched Poly(Prodrug- *Co* -Photosensitizer) Amphiphiles Unimolecular Micelles for Chemo-Photodynamic Dual Therapy, *ACS Appl. Mater. Interfaces*, 2017, **9**(42), 36675–36687, DOI: **10.1021/acsami.7b13055**.

27 M. Dionzou, A. Morère, C. Roux, B. Lonetti, J.-D. Marty, C. Mingotaud, P. Joseph, D. Goudounèche, B. Payré, M. Léonetti and A.-F. Mingotaud, Comparison of Methods for the Fabrication and the Characterization of Polymer Self-Assemblies: What Are the Important Parameters?, *Soft Matter*, 2016, **12**(7), 2166–2176, DOI: **10.1039/C5SM01863C**.

28 M. M. Modena, B. Rühle, T. P. Burg and S. Wuttke, Nanoparticle Characterization: What to Measure?, *Adv. Mater.*, 2019, **31**(32), 1901556, DOI: **10.1002/adma.201901556**.

29 J. Stetefeld, S. A. McKenna and T. R. Patel, Dynamic Light Scattering: A Practical Guide and Applications in Biomedical Sciences, *Biophys. Rev.*, 2016, **8**(4), 409–427, DOI: **10.1007/s12551-016-0218-6**.

30 H. C. Kang and Y. H. Bae, Co-Delivery of Small Interfering RNA and Plasmid DNA Using a Polymeric Vector Incorporating Endosomolytic Oligomeric Sulfonamide, *Biomaterials*, 2011, **32**(21), 4914–4924, DOI: **10.1016/j.biomaterials.2011.03.042**.

31 J. D. Ziebarth, D. R. Kennetz, N. J. Walker and Y. Wang, Structural Comparisons of PEI/DNA and PEI/SiRNA Complexes Revealed with Molecular Dynamics Simulations, *J. Phys. Chem. B*, 2017, **121**(8), 1941–1952, DOI: **10.1021/acs.jpcb.6b10775**.

32 D. Zhang, L. Wei, M. Zhong, L. Xiao, H.-W. Li and J. Wang, The Morphology and Surface Charge-Dependent Cellular Uptake Efficiency of Upconversion Nanostructures Revealed by Single-Particle Optical Microscopy, *Chem. Sci.*, 2018, **9**(23), 5260–5269, DOI: **10.1039/C8SC01828F**.

33 T. J. Thomas, H. A. Tajmir-Riahi and T. Thomas, Polyamine–DNA Interactions and Development of Gene Delivery Vehicles, *Amino Acids*, 2016, **48**(10), 2423–2431, DOI: **10.1007/s00726-016-2246-8**.

34 Y. Cheng, D. L. Sellers, J.-K. Y. Tan, D. J. Peeler, P. J. Horner and S. H. Pun, Development of Switchable Polymers to Address the Dilemma of Stability and Cargo Release in Polycationic Nucleic Acid Carriers, *Biomaterials*, 2017, **127**, 89–96, DOI: **10.1016/j.biomaterials.2017.02.036**.

35 A. Hamann, A. Nguyen and A. K. Pannier, Nucleic acid delivery to mesenchymal stem cells: a review of nonviral methods and applications, *J. Biol. Eng.*, 2019, **13**, 7, DOI: **10.1186/s13036-019-0140-0**.